

Bistatic Sensing at THz Frequencies via a Two-Stage Ultra-Wideband MIMO-OFDM System

Tommaso Bacchielli, Lorenzo Pucci, Davide Dardari, and Andrea Giorgetti

Wireless Communications Laboratory, CNIT, DEI, University of Bologna, Italy
Email: {tommaso.bacchielli2, lorenzo.pucci3, davide.dardari, andrea.giorgetti}@unibo.it

Abstract—The availability of abundant bandwidth at terahertz (THz) frequencies holds promise for significantly enhancing the sensing performance of integrated sensing and communication (ISAC) systems in the next-generation wireless systems, enabling high accuracy and resolution for precise target localization. In orthogonal frequency-division multiplexing (OFDM) systems, wide bandwidth can be achieved by increasing the subcarrier spacing rather than the number of subcarriers, thereby keeping the complexity of the sensing system low. However, this approach may lead to an ambiguity problem in target range estimation. To address this issue, this work proposes a two-stage maximum likelihood method for estimating target position in an ultra-wideband bistatic multiple-antenna OFDM-based ISAC system operating at THz frequencies. Numerical results show that the proposed estimation approach effectively resolves the ambiguity problem while achieving high resolution and accuracy target position estimation at a very low signal-to-noise ratio regime.

Index Terms—THz ISAC, bistatic sensing, two-stage ML approach, MIMO-OFDM, ultra-wideband systems.

I. INTRODUCTION

Integrated sensing and communication (ISAC) at terahertz (THz) frequencies is a key promising enabler to meet requirements for next-generation wireless systems, where the ubiquitous integration of sensing, connectivity, and intelligence across various domains will be crucial [1]. For an ISAC system, the vast bandwidth availability at THz (0.1 – 10 THz) holds the potential of exploiting ultra-wide bandwidth, leading to the simultaneous transmission of a large amount of data with unprecedented data rates [2], alongside very high range estimation accuracy and resolution [3].

Most of the studies regarding ISAC have focused on orthogonal frequency-division multiplexing (OFDM)-based systems, primarily at sub-6 GHz and millimeter wave frequencies, exploring both monostatic and bistatic radar configurations [4]–[7]. However, little investigation has been conducted to exploit the potential of ISAC system operating at THz frequencies. In [8], a novel ISAC technique with joint beam-squint and beam-split for THz massive multiple-input multiple-output (MIMO) system is presented. The authors show the advantage of the beam-squint to simultaneously transmit towards

various directions and the possibility of beam-splitting to extend sensing range and enhance accuracy using only a few subcarriers. In [9], the authors evaluate the range estimation performance of a system at THz frequencies by analyzing different waveforms. This work demonstrates that OFDM is still an excellent candidate for ISAC, also at THz, but focuses on systems with limited bandwidth, in the order of MHz.

To the author’s knowledge, there remains a lack of research investigating the potential advantages of utilizing OFDM-based ISAC systems at THz with ultra-wide bandwidth. Since the coherence bandwidth of short-range THz channels is hundreds of MHz, it is possible to achieve very high bandwidth by properly setting the subcarrier spacing without a large amount of subcarriers. However, while this solution ensures controlling the complexity, it may result in a low maximum unambiguous range, which reduces the system’s operating range [5].

In this context, this work proposes to mitigate the range estimation ambiguity problem inherent to large subcarrier spacings with a novel two-stage transmission scheme followed by a two-stage maximum likelihood (ML) estimation approach at the receiver. This approach first performs coarse target estimation over a sub-band with a smaller subcarrier spacing to avoid the ambiguity problem, followed by refined super-resolution estimation using the whole system bandwidth. Numerical results demonstrate that the proposed system can localize the target without ambiguity in a confined indoor area, ensuring cm-level range resolution and mm-level accuracy.

In this paper, we adopt the following notation: capital boldface letters for matrices, lowercase bold letters for vectors, $\text{Tr}(\cdot)$ for the trace of a matrix, $(\cdot)^*$, $(\cdot)^T$ and $(\cdot)^H$ for conjugate, transpose and conjugate transpose of a vector/matrix, respectively, and $|\cdot|$, $\|\cdot\|_2$ for the modulus and Euclidean norm, respectively. Also, \otimes , $\mathbb{E}[\cdot]$, $\text{var}[\cdot]$ for Kronecker product, statistical mean value and variance operator. $[\mathbf{X}]_{a,b,c,d}$ denotes a submatrix of \mathbf{X} composed of a subset $[a, b]$ of rows and $[c, d]$ of columns. A zero-mean circularly symmetric complex Gaussian random vector with covariance Σ is denoted by $\mathbf{x} \sim \mathcal{CN}(\mathbf{0}, \Sigma)$, while $x \sim \mathcal{U}(a, b)$ represents a uniformly distributed random variable x within the interval (a, b) .

The rest of the paper is organized as follows. In Section II and III, the system model and the proposed two-stage ML estimation method are introduced. Numerical results are presented in Section IV, while Section V concludes the paper.

This work was supported in part by the European Union under the Italian National Recovery and Resilience Plan (NRRP) of NextGenerationEU, partnership on “Telecommunications of the Future” (PE00000001 - program “RESTART”), and in part by the HORIZON-JU-SNS-2022 project TIMES (Grant Agreement Number: 101096307).

II. SYSTEM MODEL

This work considers a bistatic MIMO OFDM-based ISAC system operating at THz frequencies. In particular, for what concerns sensing, such a system consists of a transmitter (Tx) and a receiver (Rx) to form a bistatic pair. Both the Tx and the Rx are base stations (BSs) used to communicate with user equipments (UEs) or machinery while simultaneously localizing targets in the surrounding environment by using downlink signals. Differently from an ISAC monostatic system, in which a full-duplex architecture and self-interference cancellation techniques are required [4], in the bistatic configuration these problems are naturally solved as Tx and Rx are not co-located [7]. However, in this case, the Tx and the Rx need to be synchronized to perform target localization, e.g., by connecting them to a central unit that coordinates sensing operations. This work assumes that Tx and Rx are synchronized.

Without loss of generality, both Tx and Rx are equipped with a uniform linear array (ULA) composed of N_t and N_r antenna elements half-wavelength spaced, respectively. To perform sensing tasks, an OFDM frame consisting of M OFDM symbols with K active subcarriers is transmitted. The k -th subcarrier has frequency $f_k = f_c + k\Delta f$, with $k = -K/2, \dots, K/2 - 1$, where f_c is the carrier frequency and Δf the subcarrier spacing. The total frame duration is equal to MT_s , being $T_s \triangleq 1/\Delta f + T_{cp}$ the total OFDM symbol duration including the cyclic prefix (CP); the total bandwidth is therefore $B = K\Delta f$. Moreover, to exploit the ULA, beamforming is performed at the Tx through a precoding vector, \mathbf{w} .

A. Input-Output Relationship

The complex envelope of the continuous-time OFDM signal transmitted by the Tx antenna array is defined as

$$\mathbf{s}(t) = \sqrt{\frac{P_t G_t}{K}} \mathbf{w} \sum_{m=0}^{M-1} \left(\sum_{k=0}^{K-1} x[k, m] e^{j2\pi k \Delta f t} \right) g(t - mT_s) \quad (1)$$

where P_t is the total transmitted power, G_t is the single antenna element gain at the Tx, and $\mathbf{w} \in \mathbb{C}^{N_t \times 1}$ represents a unit-norm beamforming vector designed to illuminate with an almost constant gain a relatively wide angular sector where a target p is expected to be located. Moreover, $x[k, m]$ denotes a generic complex modulation symbol transmitted at time instant m on subcarrier k , while $g(t)$ represents the modulating pulse.

After the fast Fourier transform (FFT) block in the OFDM demodulator at the Rx and taking into account negligible inter-carrier interference (ICI) and inter-symbol interference (ISI), a received time-frequency grid of complex elements $y[k, m]$ is obtained at each antenna element. By aggregating the symbols at each antenna, a vector $\mathbf{y}[k, m] \in \mathbb{C}^{N_r \times 1}$ of received complex modulation symbols is obtained, as follows

$$\mathbf{y}[k, m] = \sqrt{\frac{P_t G_t G_r}{K}} \mathbf{H}_{t,r}[k, m] \mathbf{w} x[k, m] + \tilde{\mathbf{n}}[k, m] \quad (2)$$

where G_r is the single antenna element gain at the Rx, $\mathbf{H}_{t,r}[k, m] \in \mathbb{C}^{N_r \times N_t}$ is the MIMO channel matrix between

the Tx and the Rx for the subcarrier k at time m , and $\tilde{\mathbf{n}} \sim \mathcal{CN}(\mathbf{0}, \sigma_n^2 \mathbf{I}_{N_r})$ represents the additive white Gaussian noise (AWGN), with $\sigma_n^2 = N_0 \Delta f$. Here, $N_0 = k_B 290 n_F$ is the noise power spectral density, with k_B the Boltzmann constant and n_F the receiver noise figure.

B. Channel Model

Without loss of generality, this work considers a single point-like target scenario. Since a bistatic setting is considered, the channel matrix at subcarrier k and time m can be obtained as the outer product of the channel vector $\mathbf{h}_{p,r}[k, m] \in \mathbb{C}^{N_r \times 1}$, which represents the channel between the target p and the Rx, with the vector $\mathbf{h}_{t,p}[k, m] \in \mathbb{C}^{1 \times N_t}$ representing the channel between the Tx and the target p . These vectors are given by

$$\mathbf{h}_{p,r}[k, m] = \beta_{p,r} e^{j2\pi(mT_s f_{D_{p,r}} - k\Delta f \tau_{p,r})} \mathbf{b}(\theta_{p,r}) \quad (3)$$

$$\mathbf{h}_{t,p}[k, m] = \alpha_{t,p} e^{j2\pi(mT_s f_{D_{t,p}} - k\Delta f \tau_{t,p})} \mathbf{a}^H(\phi_{t,p}) \quad (4)$$

respectively. In (4), $\alpha_{t,p} = \sqrt{\xi_{t,p}} e^{-j(2\pi f_c \tau_{t,p} + \varphi_0)}$ represents the complex channel coefficient associated with target p , where $\xi_{t,p}$ denotes the channel gain, and $\varphi_0 \in \mathcal{U}[0, 2\pi)$ accounts for the phase shift between Tx and Rx. Furthermore, $\tau_{t,p} = r_{t,p}/c$ represents the propagation delay with respect to target p , where $r_{t,p}$ is the distance between target p and Tx; $f_{D_{t,p}}$ and $\phi_{t,p}$ denote the Doppler shift and angle of departure (AoD) associated with target p , respectively. The transmit array response, denoted by $\mathbf{a}(\phi_{t,p}) \in \mathbb{C}^{N_t \times 1}$, is defined considering far-field propagation conditions with the center of the array as a reference, as follows

$$\mathbf{a}(\phi_{t,p}) = \left[e^{-j\frac{N_t-1}{2}\pi \sin(\phi_{t,p})}, \dots, e^{j\frac{N_t-1}{2}\pi \sin(\phi_{t,p})} \right]^T. \quad (5)$$

When line of sight (LoS) propagation conditions are in place, the path loss coefficient is given by $\xi_{t,p} = \frac{\sigma_p}{4\pi r_{t,p}^2}$, where σ_p is the radar cross section (RCS) of target p .

Similarly, in (3), $\tau_{p,r} = \gamma_{p,r}/c$ is the propagation delay from the target p to the center of the Rx, with $\gamma_{p,r}$ the Euclidean distance between p and the Rx. Furthermore, $\beta_{p,r} = \sqrt{\zeta_{p,r}} e^{-j2\pi f_c \tau_{p,r}}$ is the channel coefficient, and $\mathbf{b}(\theta_{p,r}) \in \mathbb{C}^{N_r \times 1}$ is the array response vector defined as in (5), being $\theta_{p,r}$ the angle of arrival (AoA) related to the target p . Considering LoS propagation conditions and isotropic antenna elements with effective area $A_{\text{eff}} = c^2/(4\pi f_c^2)$, the path loss factor is given by $\zeta_{p,r} = \frac{c^2}{(4\pi f_c \gamma_{p,r})^2}$.

Starting from (3) and (4), the $N_r \times N_t$ channel matrix in (2), which represents the channel between Tx and Rx for subcarrier k at time m , can be modeled as

$$\mathbf{H}_{t,r}[k, m] = \epsilon_p e^{j2\pi(mT_s f_{D_p} - k\Delta f \tau_p)} \mathbf{b}(\theta_{p,r}) \mathbf{a}^H(\phi_{t,p}) \quad (6)$$

where $\epsilon_p = \alpha_{t,p} \beta_{p,r}$ and $\tau_p = \tau_{t,p} + \tau_{p,r}$ are the bistatic complex channel factor and bistatic propagation delay, respectively, associated with the target p . The bistatic Doppler shift f_{D_p} is defined as $f_{D_p} = f_{D_{t,p}} + f_{D_{p,r}} = \frac{2|\mathbf{v}_p|}{\lambda} \cos(\delta) \cos(\beta/2)$, where \mathbf{v}_p is the velocity of the target p , while β and δ are the bistatic angle and the angle between the velocity direction and the bisector of the bistatic angle β , respectively [7].

C. Received Signal and Signal-to-Noise Ratio

By replacing (6) in (2) and stacking the $K \times M$ transmitted symbol grid into a $KM \times 1$ vector $\underline{\mathbf{x}}$, a more compact form of the vector of received symbols $\underline{\mathbf{y}} \in \mathbb{C}^{N_r KM \times 1}$ can be obtained as follows

$$\underline{\mathbf{y}} = \sqrt{\frac{P_t G_t G_r}{K}} \epsilon_p \mathbf{G}(f_{D_p}, \tau_p, \theta_{p,r}, \phi_{t,p}) \underline{\mathbf{x}} + \underline{\mathbf{n}} \quad (7)$$

where $\mathbf{G}(\cdot)$ is the effective channel matrix of dimension $N_r KM \times KM$, defined for a generic target p , as

$$\mathbf{G}(f_{D_p}, \tau_p, \theta_{p,r}, \phi_{t,p}) \triangleq \mathbf{T}(\tau_p, f_{D_p}) \otimes (\mathbf{b}(\theta_{p,r}) \mathbf{a}^H(\phi_{t,p}) \mathbf{w}) \quad (8)$$

with $\mathbf{T}(\tau_p, f_{D_p}) \in \mathbb{C}^{KM \times KM}$ defined as

$$\mathbf{T}(\tau_p, f_{D_p}) \triangleq \text{diag}\left([1, \dots, e^{j2\pi(M-1)T_s f_{D_p}}]^T \otimes [1, \dots, e^{-j2\pi(K-1)\Delta f \tau_p}]^T\right) \quad (9)$$

Recalling the complex channel factor ϵ_p and the noise variance σ_n^2 introduced in Section II-B, the signal-to-noise ratio (SNR) of the bistatic radar system related to target p can be defined as

$$\begin{aligned} \text{SNR} &= \frac{\mathbb{E}\{|x[k, m]|^2\} P_t G_t^a G_r |\epsilon_p|^2}{K \sigma_n^2} \quad (10) \\ &= \mathbb{E}\{|x[k, m]|^2\} \frac{P_t G_t^a G_r \sigma_p c^2}{(4\pi)^3 r_{t,p}^2 \gamma_{p,r}^2 f_c^2 N_0 K \Delta f}. \end{aligned}$$

where G_t^a is the total Tx antenna array gain in the direction of p , considering both G_t and beamforming gain. If convenient, when performing numerical simulations varying the SNR, (10) can be recast as $\text{SNR} = 1/\sigma_n^2$, by normalizing the transmitted complex symbols to average unit transmit power as $\mathbb{E}\{|x[k, m]|^2\} = 1$ and setting $|\epsilon_p|^2 = 1$.

D. Target Position Estimation

In this work, the bistatic propagation delay τ_p , which is directly related to the bistatic range $r_p = \tau_p c$, and the AoA θ_p , are estimated via a ML approach.

As already mentioned, at Tx we perform beamforming through a vector \mathbf{w} designed to provide nearly constant gain over a wide circular sector. Therefore, at the Rx, the array response from Tx to the target is a complex constant, i.e., $g_p = \mathbf{a}^H(\phi_p) \mathbf{w}$, which can be absorbed in the channel gain coefficient, as $h_p \triangleq g_p \epsilon_p$. The effective channel gain thus becomes independent on the AoD ϕ_p , i.e., $\mathbf{G}(f_{D_p}, \tau_p, \theta_p)$.

The vector of sensing parameters related to the target p to be estimated is defined as $\Theta_p = (|h_p|, \angle h_p, f_{D_p}, \tau_p, \theta_p)$, so the ML estimate of the set Θ_p involves a search in the space $\Gamma \triangleq \mathbb{C} \times \mathbb{R}^3$ [10]

$$\Theta_{\text{ML}} = \arg \min_{\Theta_p \in \Gamma} \left\| \underline{\mathbf{y}} - \sqrt{\frac{P_t G_t G_r}{K}} h_p \mathbf{G}(f_{D_p}, \tau_p, \theta_p) \underline{\mathbf{x}} \right\|_2^2 \quad (11)$$

One possible solution of (11) can be obtained through a generalized maximum likelihood (GML) approach. It consists

of estimating the sensing parameters of interest in Θ_p by maximizing the log-likelihood function with respect to the channel gain coefficient h . This reduces the sensing parameters ML estimation to the solution of the following problem

$$\left(\hat{f}_{D_p}, \hat{\tau}_p, \hat{\theta}_p \right) = \arg \max_{(f_D, \tau, \theta) \in \Psi} \frac{|\boldsymbol{\xi}(\tau, f_D) \mathbf{b}^*(\theta)|^2}{\underline{\mathbf{x}}^H \mathbf{b}^H(\theta) \mathbf{b}(\theta) \underline{\mathbf{x}}} \quad (12)$$

where Ψ is a grid composed of a set of (f_D, τ, θ) tuples, and $\boldsymbol{\xi}(\tau, f_D) = [\underline{\mathbf{x}}^H \mathbf{T}^H(\tau, f_D) \mathbf{Y}^T]^T$, with $\mathbf{Y} = [\underline{\mathbf{y}}_1[0, 0], \dots, \underline{\mathbf{y}}_{N_r}[M-1, K-1]] \in \mathbb{C}^{N_r \times KM}$. The position of the target p is thus obtained from the estimate of the bistatic range $\hat{r}_p = \hat{\tau}_p c$ and AoA $\hat{\theta}_p$, by first computing the distance from target p to Rx, as

$$\hat{\gamma}_p = \frac{\hat{r}_p^2 - L^2}{2(\hat{r}_p + L \sin(\hat{\theta}_p - \pi/2))} \quad (13)$$

where L is the distance between Tx and Rx, commonly referred to as *baseline*. Then, the estimated position of the target with respect to the Rx is $\hat{\mathbf{p}}_p = [\hat{\gamma}_p \cos(\hat{\theta}_p), \hat{\gamma}_p \sin(\hat{\theta}_p)]^T$.

E. Position Error Bound

Let us consider the received signal in (7), and define $\underline{\mathbf{s}} = \sqrt{\frac{P_t G_t G_r}{K}} h_p \mathbf{G}(f_{D_p}, \tau_p, \theta_p) \underline{\mathbf{x}} \in \mathbb{C}^{N_r KM \times 1}$ as the vector of mean values of $\underline{\mathbf{y}}$. The Cramér-Rao lower bound (CRLB) on the estimation of the unknown parameters in Θ_p is

$$\text{var}[\hat{\Theta}_{p_i}] \geq \text{CRLB}(\hat{\Theta}_{p_i}) = I_{p_{ii}}^{-1} \quad i = 1, \dots, \text{card}(\Theta_p) \quad (14)$$

where $\hat{\Theta}_{p_i}$ is the estimate of the i -th parameter contained in Θ_p , and $I_{p_{ii}}^{-1}$ represents the i -th element on the main diagonal of the inverse of the Fisher information matrix (FIM) \mathbf{I}_p . The generic ij -th element of \mathbf{I}_p can be computed as [11], [12]

$$I_{p_{ij}} = \frac{2}{\sigma_n^2} \Re \left\{ \sum_{k,m,n} \left(\frac{\partial s_n[k, m]}{\partial \Theta_{p_i}} \right)^* \left(\frac{\partial s_n[k, m]}{\partial \Theta_{p_j}} \right) \right\} \quad (15)$$

where $s_n[k, m]$ is the (n, k, m) element of a 3D array obtained starting from the $N_r KM \times 1$ vector $\underline{\mathbf{s}}$ and given by

$$s_n[k, m] = \sqrt{\frac{P_t G_t G_r}{K}} h_p e^{j2\pi(m T_s f_{D_p} - k \Delta f \tau_p)} b_n(\theta_p) x[k, m] \quad (16)$$

being $b_n(\theta_p)$ the n -th element of the array response vector \mathbf{b} . After computing the inverse of the FIM \mathbf{I}_p , the bound on position estimation accuracy, hereinafter referred to as position error bound (PEB), is given by $\text{PEB} = \sqrt{\text{CRLB}(\hat{\mathbf{p}}_p)}$, where the CRLB of position estimate can be found as [13]

$$\begin{aligned} \text{CRLB}(\hat{\mathbf{p}}_p) &= \text{Tr}(\mathbf{J}_\Omega^{-1} [\mathbf{I}_p^{-1}(\Theta_p)]_{4:5,4:5} [\mathbf{J}_\Omega^{-1}]^T) \\ &= \text{Tr}([\mathbf{I}_p^{-1}(\Theta)]_{4:5,4:5} [\mathbf{J}_{\Omega^{-1}}]^T \mathbf{J}_{\Omega^{-1}}) \quad (17) \end{aligned}$$

being \mathbf{J}_Ω the Jacobian of the transformation $\Omega : \hat{\mathbf{p}}_p = (x_p, y_p) \rightarrow (\tau_p, \theta_p)$, and $\mathbf{J}_{\Omega^{-1}}$ the Jacobian of the inverse transformation $\Omega^{-1} : (\tau_p, \theta_p) \rightarrow \hat{\mathbf{p}}_p = (x_p, y_p)$, defined as¹

$$\mathbf{J}_{\Omega^{-1}} = \begin{bmatrix} \frac{\partial x_p}{\partial \tau_p} & \frac{\partial x_p}{\partial \theta_p} \\ \frac{\partial y_p}{\partial \tau_p} & \frac{\partial y_p}{\partial \theta_p} \end{bmatrix}. \quad (18)$$

¹Note that the following property holds $\mathbf{J}_{\Omega^{-1}} = \mathbf{J}_\Omega^{-1}$, and vice versa.

III. TWO-STAGE METHOD FOR AMBIGUITY PROBLEM MANAGEMENT

The advantage of using huge bandwidths at THz is beneficial for both the communication and the sensing functionalities of the OFDM-based ISAC system. From a communication viewpoint, wider bandwidths increase channel capacity and enhance robustness by exploiting multipath propagation. In contrast, for what concerns the sensing part, larger bandwidths enable higher range resolution, making it possible to distinguish targets that may be very close to each other. In fact, an OFDM system with a bandwidth of the order of GHz can achieve cm-level range resolution, according to $r_{\text{res}} = c/B$, for a bistatic configuration. Moreover, a larger bandwidth also increases performance in terms of root mean square error (RMSE) on position estimation, with a lower PEB. Increasing the subcarrier spacing Δf seems a natural choice to increase the bandwidth without compromising system complexity, especially when a ML estimation approach is considered.

It's important to note that while increasing Δf is feasible at THz due to the coherence band being of the order of hundreds of MHz [14], it can lead to an ambiguity problem in target position estimation. This problem persists even in relatively small areas, as the maximum unambiguous range, in these conditions, is less than the maximum distance that can be estimated in the area of interest. For instance, the maximum unambiguous bistatic range in an OFDM-based radar is $r_{\text{unamb}} = c/\Delta f$. To solve this problem, which can cause the impossibility of correctly estimating the target position, a two-stage ML estimation algorithm is proposed in this work. The approach consists of a novel two-stage transmission scheme and a two-stage ML estimation approach at the receiver. In the first phase, a coarse target estimation exploits a transmitting signal that uses a sub-band with narrow subcarrier spacing to avoid the ambiguity problem. Then, in the second phase, the transmission exploits the full system bandwidth, and at the receiver, a refined super-resolution estimation is performed around the coarse estimate.

The considered OFDM ISAC system operates over a large bandwidth B , of the order of GHz, with a large number of equispaced subcarriers K and subcarrier spacing Δf , in the order of few MHz. However, such a system manages the complexity using a relatively small number K' of active subcarriers out of the K available, as shown in Fig. 1. The remaining subcarriers can be used for communication purposes. The two phases are summarized below.

- **Coarse target estimation:** Localization of target p with coarse resolution over a search area A by using a sub-band B_{coarse} of the system bandwidth B around the carrier frequency f_c , with K' contiguous active subcarriers within B_{coarse} and considering a subcarrier spacing Δf . The ML target position estimation according to (12) is performed without range ambiguity by properly designing B_{coarse} such that $B_{\text{coarse}} \leq (cK)/r_{\text{unamb}}$, where r_{unamb} is the maximum unambiguous bistatic range compatible with the search area A .

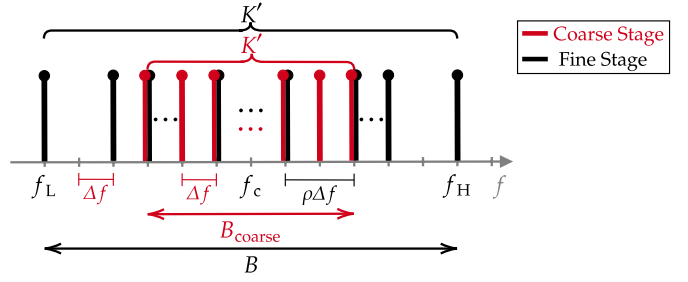


Figure 1: Illustration of the proposed two-stage method with $\rho = 2$.

- **Fine target estimation:** Localization of target p with refined resolution and without range ambiguity around the target position estimated in the coarse stage. Here, the system uses the same number K' of properly equispaced active subcarriers out of the K over the overall bandwidth B , with $\rho\Delta f$ subcarrier spacing, where $\rho \triangleq B/B_{\text{coarse}}$. The search interval² is centered in the target position estimated in the previous stage, and the width of the bistatic range search interval must be less than double the maximum unambiguous range, by considering the system working on the overall bandwidth B , i.e., $< 2r_{\text{unamb}} = (2cK)/B$. Again, the ML approach in (12) is here used for target position estimation.

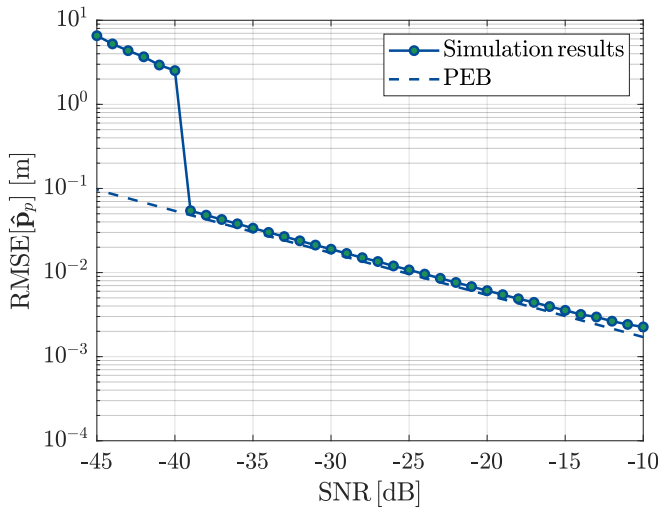
This way, the proposed system can exploit an ultra-wide bandwidth at THz to achieve highly precise and unambiguous range localization while maintaining low system complexity.

IV. NUMERICAL RESULTS

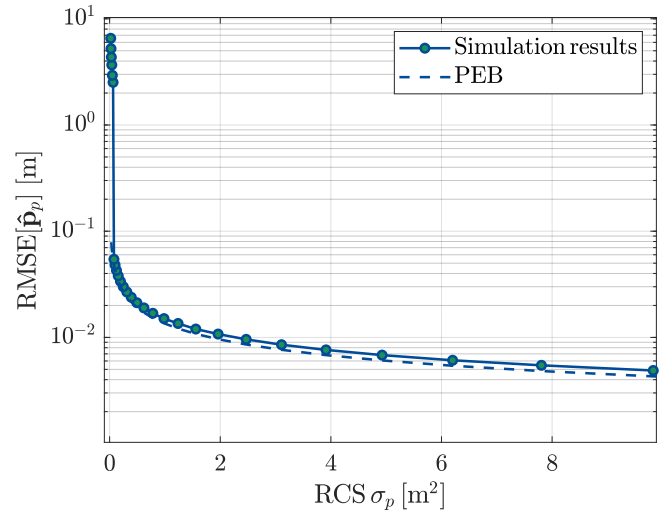
Numerical simulations are performed to evaluate the sensing performance of the proposed two-stage ultra-wideband system at THz frequencies. In particular, we consider $f_c = 0.3$ THz, $B = 2$ GHz, $B_{\text{coarse}} = 400$ MHz, $\Delta f = 6.25$ MHz, $K = 320$, $K' = 64$, $M = 50$, $N_t = N_r = 64$, $P_t G_t^a = 1$ W, $G_r = 1$, $N_0 = 4 \cdot 10^{-20}$ W/Hz, and $\rho = 5$. The cyclic prefix duration has been set to $T_{\text{cp}} = 19.5$ ns, according to the channel delay spread, here approximated as $T_{\text{cp}} = (r_{\text{bis,max}} - L)/c$, where $r_{\text{bis,max}}$ is the maximum bistatic range within the considered squared area A of 10×10 m². In addition, quadrature phase shift keying (QPSK) constellation, and a scenario as the one described in Section II are considered. The target p is assumed to be stationary (i.e., $|\mathbf{v}_p| = 0$), inside the designated area and located at a distance of 7.9 m from both Tx and Rx units, with $\phi_p = 18.4^\circ$ and $\theta_p = -26.5^\circ$ as AoD and AoA, respectively, with the Tx and Rx placed in the bottom left and top right corners of the area.

The analysis is performed through curves of RMSE of target position estimation $\hat{\mathbf{p}}_p$ and PEB as a function of the SNR and target RCS σ_p . When the SNR is varied, this is normalized as explained in Section II-C. Conversely, when σ_p is varied the considered SNR is given according to (10), as a function of σ_p , \mathbf{p} , and the system parameters above.

²Note that, the search interval width should be properly set, e.g., by considering the PEB of the coarse stage, computed according to Section II-E.



(a) RMSE of target p position estimation and PEB vs SNR



(b) RMSE of target p position estimation and PEB vs RCS σ_p

Figure 2: RMSE compared to the PEB related to position estimation $\hat{\mathbf{p}}_p$ of target p as a function of SNR (a) and RCS σ_p (b), considering $r_{t,p} = r_{p,r} = 7.9$ m, $\phi_p = 18.4^\circ$, $\theta_p = -26.5^\circ$, and $|\mathbf{v}_p| = 0$ km/h as target parameters.

The obtained results are shown in Fig. 2. In particular, in Fig. 2a, it can be observed that the considered ISAC system with the proposed two-stage ML estimation method, exhibits good position estimation performance up to SNR = -39 dB, where the RMSE curve related to the target position estimation $\hat{\mathbf{p}}_p$ nearly coincides with the PEB curve. The possibility of correctly estimating the target in correspondence with extremely low values of SNR is especially valuable at THz, where the path loss significantly affects the performance. Furthermore, it is worth noting that such a system can reach a mm accuracy on the position estimation, without range ambiguities, for values of SNR greater than -10 dB, under the above simulation parameters and conditions. Note that the bistatic range resolution is 15 cm, thanks to the use of a $B = 2$ GHz bandwidth. In Fig. 2b, the RMSE on position estimation $\hat{\mathbf{p}}_p$ is plotted as a function of the RCS of the target. As it can be observed, the proposed two-stage ISAC system can correctly estimate, with sub-cm accuracy, the position of the target with an RCS approximately greater than 1 m² at a distance of 7.9 m from both the Tx and Rx, showing performance very close to the theoretical bound.

V. CONCLUSION

This work introduced a two-stage ML-based estimation approach for managing range ambiguity in a bistatic MIMO-OFDM ISAC system at THz frequencies that use a GHz-wide bandwidth. Initially, a coarse target position is estimated using a small sub-band to avoid ambiguity within the monitored area. The estimation is then refined using the system's full bandwidth to enhance position accuracy and resolution. The approach maintains low computational complexity and uses a small fraction of the subcarriers to save resources for communication. Numerical results confirm that the method effectively resolves range ambiguity, achieving near-optimal RMSE performance even at very low SNR regimes.

REFERENCES

- [1] W. Tong and P. Zhu, *6G: The Next Horizon: From Connected People and Things to Connected Intelligence*. Cambridge University Press, 2021.
- [2] A. Hrovat *et al.*, "Integrated communications and sensing in terahertz band: A propagation channel perspective," *J. Commun. Softw. Syst.*, vol. 20, no. 1, pp. 23–37, 1 2024.
- [3] W. Jiang *et al.*, "Terahertz communications and sensing for 6g and beyond: A comprehensive review," *IEEE Commun. Surveys Tuts.*, 2024.
- [4] C. B. Barneto *et al.*, "Full-duplex OFDM radar with LTE and 5G NR waveforms: challenges, solutions, and measurements," *IEEE Trans. Microw. Theory Techn.*, vol. 67, no. 10, pp. 4042–4054, Oct. 2019.
- [5] M. Braun, "OFDM radar algorithms in mobile communication networks," Ph.D. dissertation, Karlsruhe Institute of Technology, 2014.
- [6] L. Pucci, E. Paolini, and A. Giorgetti, "System-level analysis of joint sensing and communication based on 5G new radio," *IEEE J. Sel. Areas Commun.*, vol. 40, no. 7, pp. 2043–2055, July 2022.
- [7] L. Pucci, E. Matricardi, E. Paolini, W. Xu, and A. Giorgetti, "Performance analysis of a bistatic joint sensing and communication system," in *IEEE Int. Conf. on Commun. Work.*, Seoul, Republic of Korea, May 2022, pp. 73–78.
- [8] F. Gao, L. Xu, and S. Ma, "Integrated sensing and communications with joint beam-squint and beam-split for mmwave/THz massive MIMO," *IEEE Trans. Commun.*, vol. 71, no. 5, pp. 2963–2976, 2023.
- [9] C. Han, Y. Wu, Z. Chen, Y. Chen, and G. Wang, "THz ISAC: A physical-layer perspective of terahertz integrated sensing and communication," *IEEE Commun. Mag.*, vol. 62, no. 2, pp. 102–108, 2024.
- [10] S. K. Dehkordi, L. Pucci, P. Jung, A. Giorgetti, E. Paolini, and G. Caire, "Multi-static parameter estimation in the near/far field beam space for integrated sensing and communication applications," 2023. [Online]. Available: <https://arxiv.org/abs/2309.14778>
- [11] D. Rife and R. Boorstyn, "Single tone parameter estimation from discrete-time observations," *IEEE Trans. Inf. Theory*, vol. 20, no. 5, pp. 591–598, 1974.
- [12] T. Bacchielli, L. Pucci, E. Paolini, and A. Giorgetti, "Performance analysis of a low-complexity OTFS integrated sensing and communication system," in *IEEE Vehicular Technology Conference*, Hong Kong, Hong Kong, Oct. 2023.
- [13] D. B. Jourdan, D. Dardari, and M. Z. Win, "Position error bound for UWB localization in dense cluttered environments," *IEEE Trans. Aerosp. Electron. Syst.*, vol. 44, no. 2, pp. 613–628, 2008.
- [14] I. F. Akyildiz, C. Han, Z. Hu, S. Nie, and J. M. Jornet, "Terahertz band communication: An old problem revisited and research directions for the next decade," *IEEE Trans. Commun.*, vol. 70, no. 6, pp. 4250–4285, 2022.